Chapter 2

Sound velocities of $(Mg_{0.16}Fe_{0.84})O$ measured by Nuclear Resonant Inelastic X-Ray Scattering*

* *This chapter has been previously published as: Wicks, J. K., J. M. Jackson, and W. Sturhahn (2010), Very low sound velocities in iron-rich (Mg,Fe)O: Implications for the core-mantle boundary region, Geophys. Res. Lett., 37, L15304. A re-evaluation of this data is briefly discussed in Chapter 5*

2.1 Nuclear Resonant Scattering

Nuclear resonant scattering (NRS) methods take advantage of the fact that nuclei, much like electrons, can be excited into higher energy states, which are organized into discrete energy levels. A resonance energy is the energy that corresponds to the excitation of a nucleus into one of these higher energy levels, at which energy the absorption cross-section of the nucleus is much higher. Whether a nucleus is accessible for nuclear resonant studies is a function of both nuclear excitation energy and lifetime of the excited state. We refer the reader to references such as *Sturhahn* (2004) that introduce the spectroscopy technique and *Sturhahn* (2000) that describes the software. In addition, *Sturhahn and Jackson* (2007) discusses NRS techniques in the context of geophysical application.

2.1.1 Nuclear Resonant Inelastic X-Ray Scattering (NRIXS)

Nuclear resonant inelastic X-ray scattering (NRIXS) is a technique that probes the lattice vibrations in which the resonant atoms participate. It is complementary to techniques such as Raman spectroscopy and infrared spectroscopy in that it measures vibrations of a lattice, but differs in both information and execution. Most notably, there are no selection rules for NRIXS, so no vibrations are missed based on symmetry. However, because it is isotope-specific, the vibrations measured are a projection of lattice vibrations onto the resonant isotope.

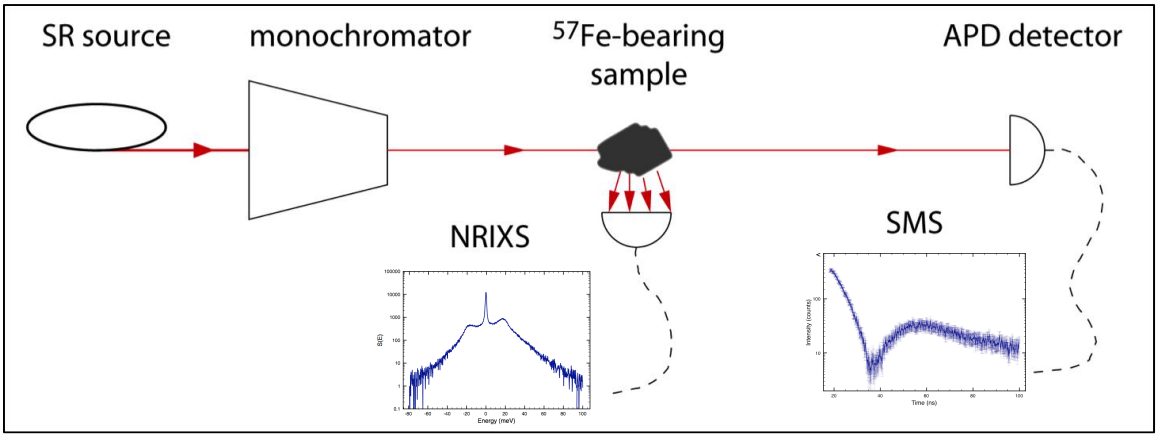

Figure 2.1: Setup of Nuclear Resonant Scattering measurements at Sector 3-ID-B of the Advanced Photon Source. Figure adapted from (*Sturhahn and Jackson*, 2007).

Figure 2.1 shows a cartoon of the setup of nuclear resonant scattering measurements at Sector 3-ID-B of the Advanced Photon Source (APS). The synchrotron radiation (SR) of the APS is a third-generation light source capable of producing X-rays with high flux and brilliance. In Sector 3 of the APS a series of monochromators eliminate all energies except the resonance energy with a 1 meV bandwidth. In the case of ^{57}Fe, the resonance energy is 14.4125 keV, and the energies corresponding to inelastic scattering are obtained by tuning the energy around the resonance peak. Incoherent scattering is measured radially as close to the sample as possible using avalanche photodiodes detectors (APDs), and produce the NRIXS spectra. Coherent scattering is measured in the forward direction, further downstream, which gives us the shape of the elastic peak, which reflects the source, and the synchrotron Mössbauer spectrum if measured in the time domain.

Figure 2.2 shows an example energy scan collected in an NRIXS experiment. The elastic peak

at the origin corresponds to recoilless absorption and emission. Peaks on either side of the elastic peak correspond to phonon annihilation (anti-Stokes) or creation (Stokes). The spectrum measured in the forward direction gives the shape of the elastic peak, and is scaled and subtracted from the NRIXS spectrum to isolate the vibrations.

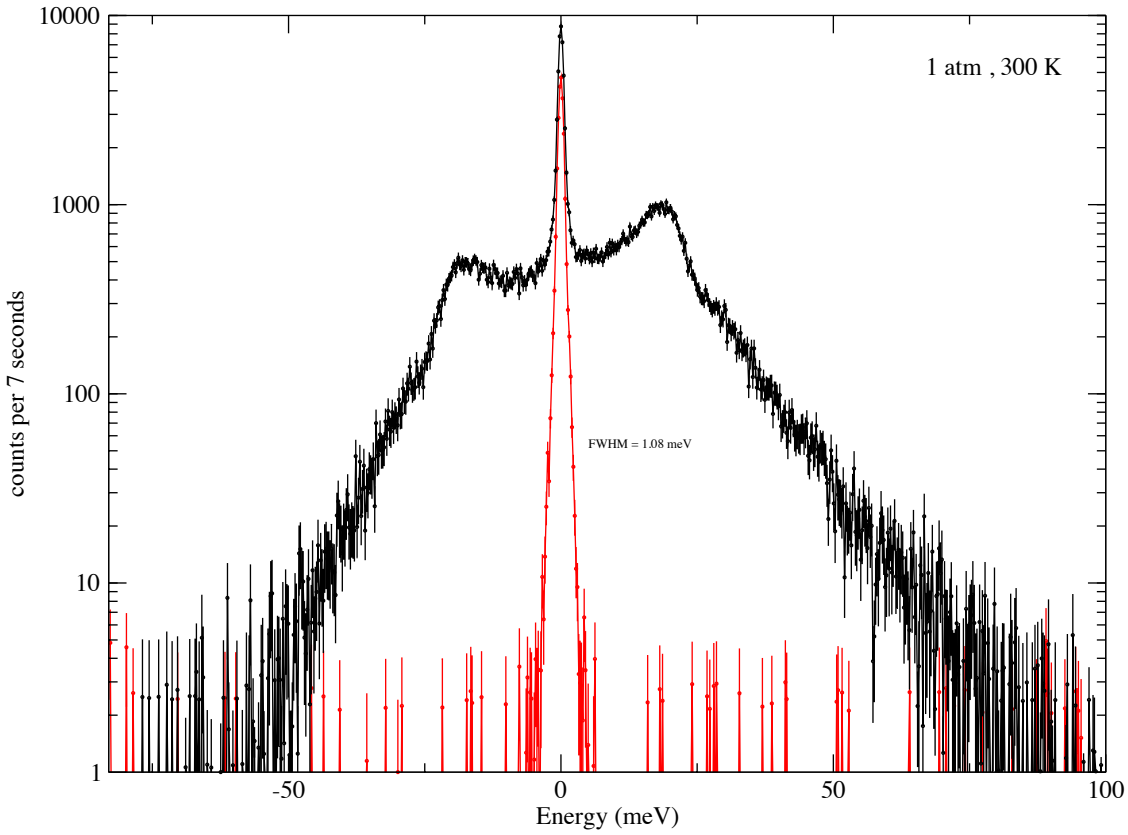

Figure 2.2: Sample energy scan (raw NRIXS spectrum) of $(Mg_{.06}Fe_{.94})O$ around the ^{57}Fe resonance energy of 14.4125 keV at ambient pressure and temperature. The spectrum independently measured in the forward direction gives the shape of the elastic peak (red). The spectrum measured radially captures the inelastic absorptions corresponding to lattice vibrations (black).

2.1.2 Synchrotron Mössbauer Spectroscopy (SMS)

Mössbauer spectroscopy measures small changes to nuclear energy levels in response to its environment. From this technique, we gain information about the electronic and magnetic environment of a nucleus that has an accessible resonance (e.g. ^{57}Fe).

Nuclear energy levels are sensitive to the electric field gradient, which couples with the quadrupole

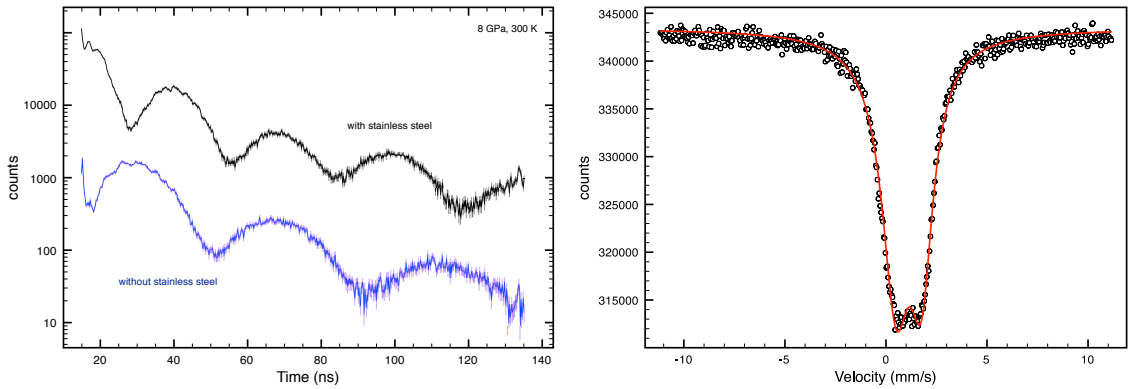

Figure 2.3: Left: Synchrotron Mössbauer spectra of $(Mg_{.06}Fe_{.94})O$ at 8 GPa, with and without stainless steel reference. Right: Conventional Mössbauer spectrum of $(Mg_{.06}Fe_{.94})O$ at 0 GPa, with a fit drawn in red corresponding to a quadrupole splitting of 1 mm/s and isomer shift of 0.8 mm/s, consistent with divalent iron.

moment of the nucleus. An asymmetric electronic distribution around the nucleus, then, results in quadrupole splitting. Nuclear energy levels split even further in the presence of electric or magnetic fields. Synchrotron Mössbauer spectroscopy measures the Rayleigh scattering of excited resonant nuclei, where a superposition of different emitted energies reflecting nuclear level splitting can be measured using detectors as a function of time.

Figure 2.3 shows an example of typical Mössbauer spectra of $(Mg_{.06}Fe_{.94})O$ at low pressures. Higher pressure data is discussed in Chapter 3. A quadrupole splitting of energy manifests as a split peak in conventional spectra (right), and as an oscillational frequency in synchrotron Mössbauer spectra (left). In conventional spectra, the isomer shift measured gives the energy shift of the ground energy level with respect to the gamma ray source, typically ^{57}Co embedded in stainless steel. In synchrotron Mössbauer spectroscopy, isomer shift is determined by measuring a sample twice, with and without a reference absorber in the beam. Advantages of synchrotron Mössbauer spectroscopy over conventional methods include no source broadening, no background, and high photon flux at the resonance energy of the ^{57}Fe atom, permitting high quality spectra with reasonable count times of samples even at high pressure.

2.2 Experiments and Data Evaluation

The $(Mg_{.16}{}^{57}Fe_{.84})O$ sample was synthesized at room pressure in a gas-mixing furnace. Details of synthesis and purity can be found in section A.1. Three panoramic diamond anvil cells (DACs) were prepared for this experiment. The panoramic DACs were designed and machined at Caltech. Beveled anvils with 250 and 300 μm-flat culet diameters were used. A 140 μm sample chamber was drilled out of a pre-indented beryllium gasket for each DAC, and the sample was loaded in the center of a boron epoxy insert to increase sample thickness, aid in gasket stability, and reduce pressure gradients. In one of the three DAC setups, a NaCl pressure medium was included with the sample, and no boron epoxy was used. Small ruby spheres were loaded close to the sample in all DACs to determine pressure before and after data collection using the characteristic ruby fluorescence line shift according to the non-hydrostatic ruby pressure scale (*Mao et al.*, 1978).

High-pressure nuclear resonance scattering experiments were conducted at Sector 3-ID-B of the Advanced Photon Source at Argonne National Laboratory (*Sturhahn and Jackson*, 2007, Figure 2.1). The storage ring was operated in top-up mode with 24 bunches separated by 153 ns. The X-ray energy incident on the sample had a bandwidth of 1.2 meV and was tuned around the 14.4125 keV nuclear resonance of ^{57}Fe (*Toellner et al.*, 2001). Time-delayed photons resulting from nuclear excitation of the ^{57}Fe isotope in $(Mg_{.16}Fe_{.84})O$ were collected using three avalanche photodiode detectors (APDs) positioned radially around the DAC. At each pressure, inelastically scattered photons were collected over select energy ranges spanning -80 meV to +100 meV. Nuclear resonance inelastic X-ray scattering (NRIXS) spectra were collected from ambient pressure to 121 GPa at 300 K. Raw spectra are shown in Figure 2.4.

From the measured energy spectra, the partial projected phonon density of states (PDOS) pertaining to the Fe site was extracted using methods described in (*Sturhahn*, 2004). PDOSs are shows in Figure 2.5.

A fourth APD was positioned in the forward direction with two goals: 1) to measure the resolution function independently for accurate sound velocity determination and 2) to measure the time spectra using synchrotron Mössbauer spectroscopy for local magnetic environment determination of the ^{57}Fe

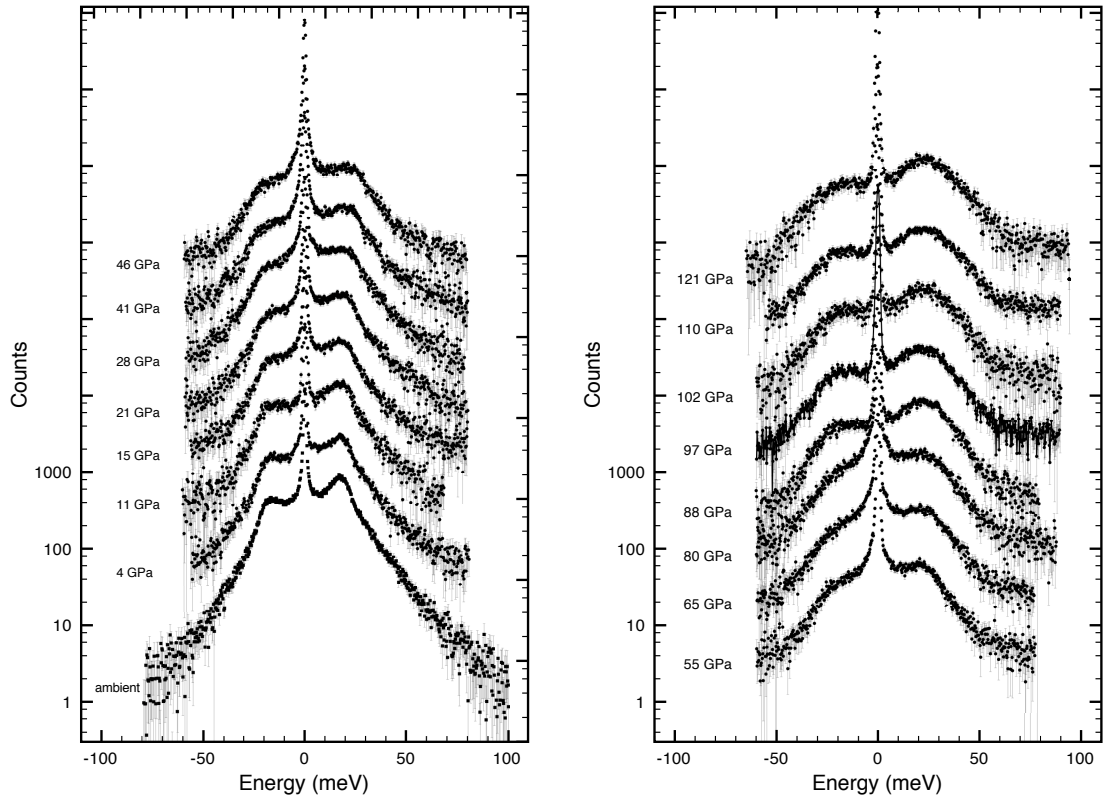

Figure 2.4: Raw NRIXS spectra of $(Mg_{.16}Fe_{.84})O$ at 300 K at different pressures over 0 to 120 GPa, measured at Sector 3-ID-B of the Advanced Photon Source. They are offset in the y-direction for clarity.

(Figure 2.6).

The Debye sound velocity, V_D, is related to the low-energy region of the PDOS in the following manner:

$$V(E) = \left\{ \frac{m\,E^2}{2\pi^2\hbar^3\rho\,D(E)} \right\}^{\frac{1}{3}} \quad \text{and} \quad V_D = V(0) \ , \tag{2.1}$$

where m is the mass of the resonant nucleus, ρ is the mass density of the sample, and $D(E)$ is the PDOS. Values of $V(E)$ were calculated from the measured PDOS and matched to an empirical function $f(E) \approx V_D\,\{1-(E/E_0)^2\}$, where E_0 and V_D are optimized in a standard least-square-fit procedure (*Jackson et al.*, 2009). The energy region for the fit was chosen between 4 and 14 meV.

The lower limit of the energy range is chosen to avoid errors resulting from the subtraction of the elastic contributions and is mainly determined by the energy bandwidth of the X-rays. The upper limit is chosen as the maximum possible energy that permits an acceptably small χ^2 value in

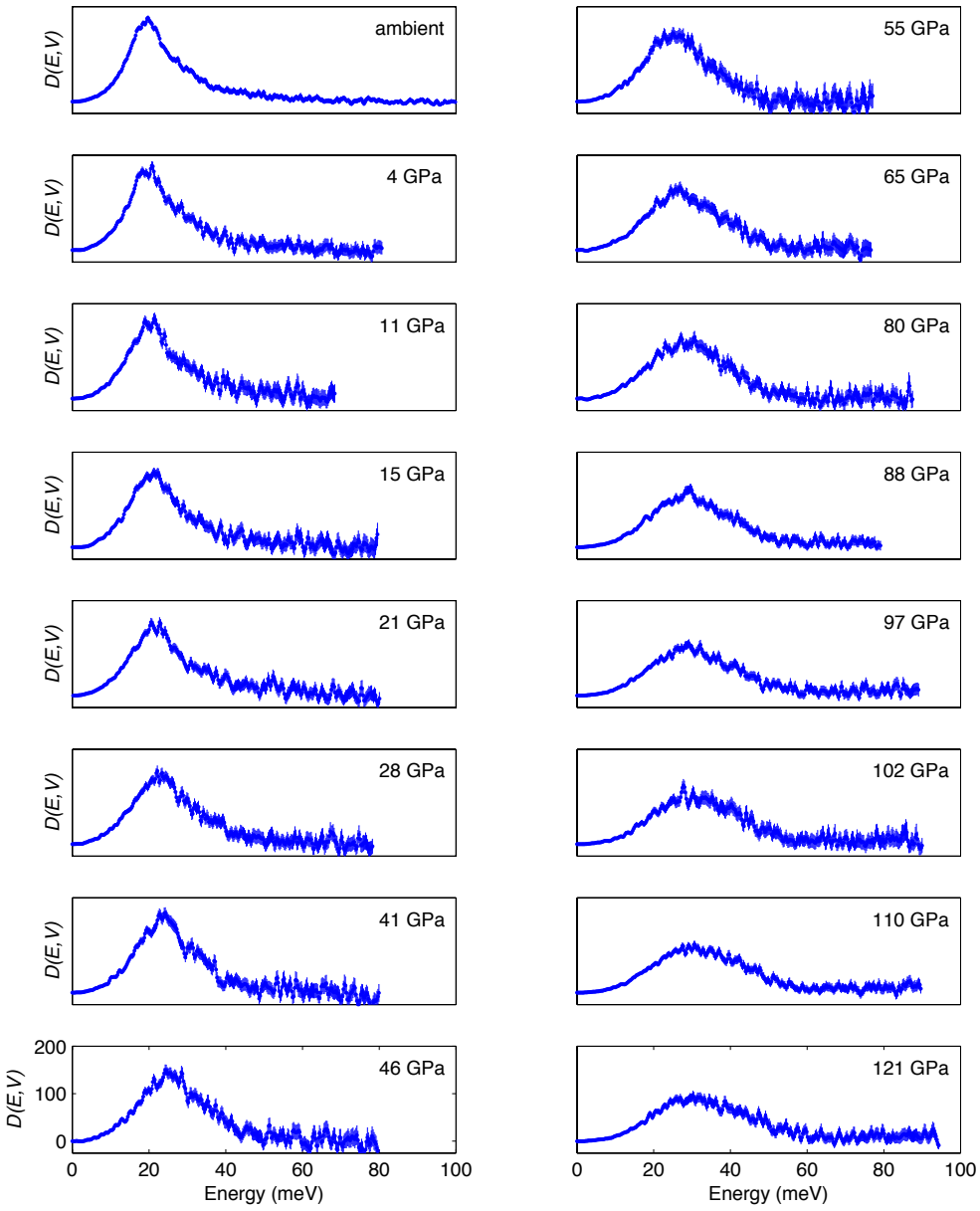

Figure 2.5: Partial projected phonon density of states (PDOSs) of $(Mg_{.16}Fe_{.84})O$, extracted from the NRIXS scans using the PHOENIX software.

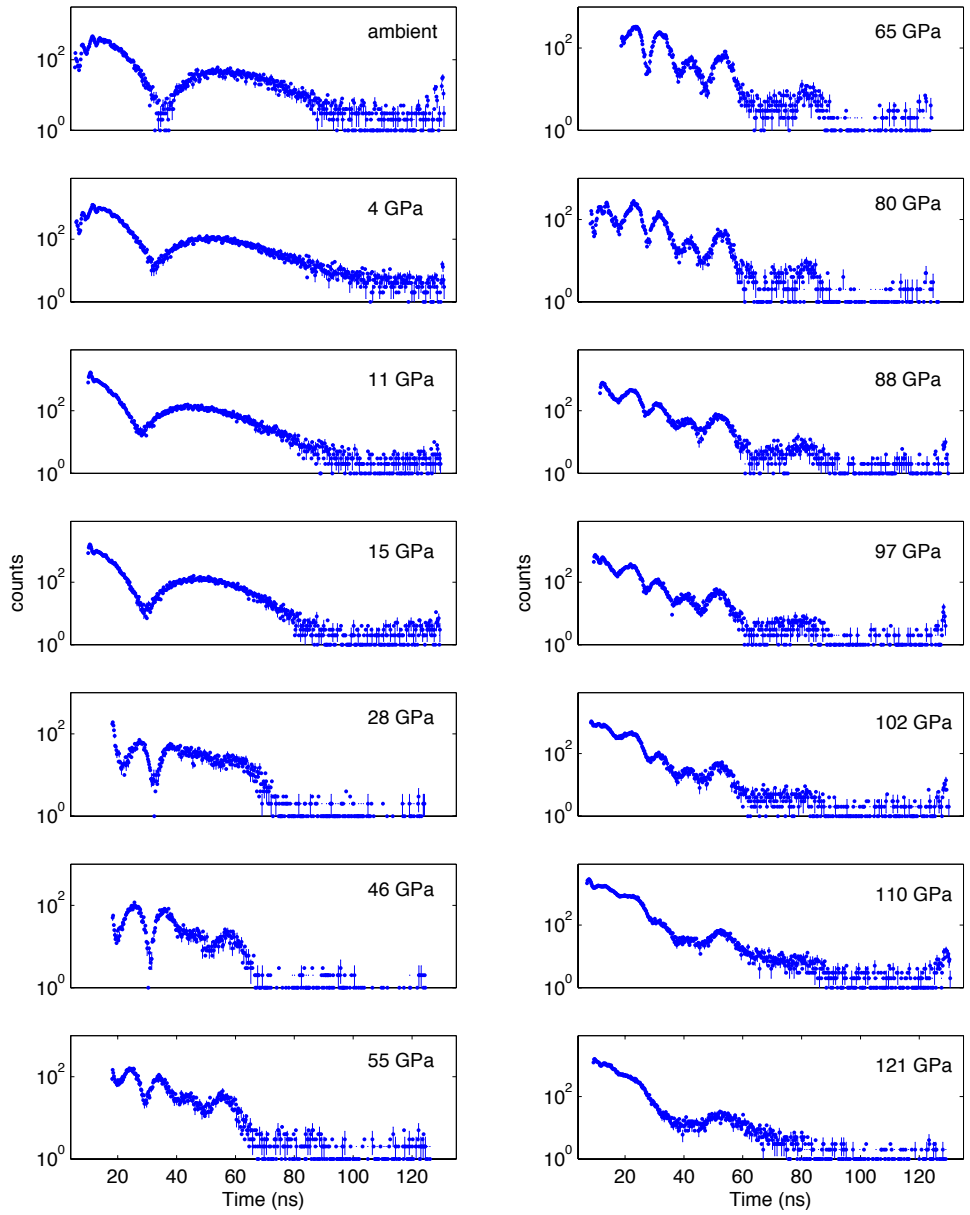

Figure 2.6: Time spectra of $(Mg_{.16}Fe_{.84})O$ from synchrotron Mössbauer spectroscopy. The ambient pressure spectrum is characterized by slow oscillations, consistent with no magnetic ordering. Fast oscillations appear in the spectrum at 28 GPa. A magnetically-ordered state is stable between 28 and 110 GPa. At 121 GPa, the fast oscillations have disappeared, which is indicative of a spin transition to a low-spin state of the Fe $3d$-electron configuration. Error bars are shown for every fourth point, and each data point represents a binning of 4.

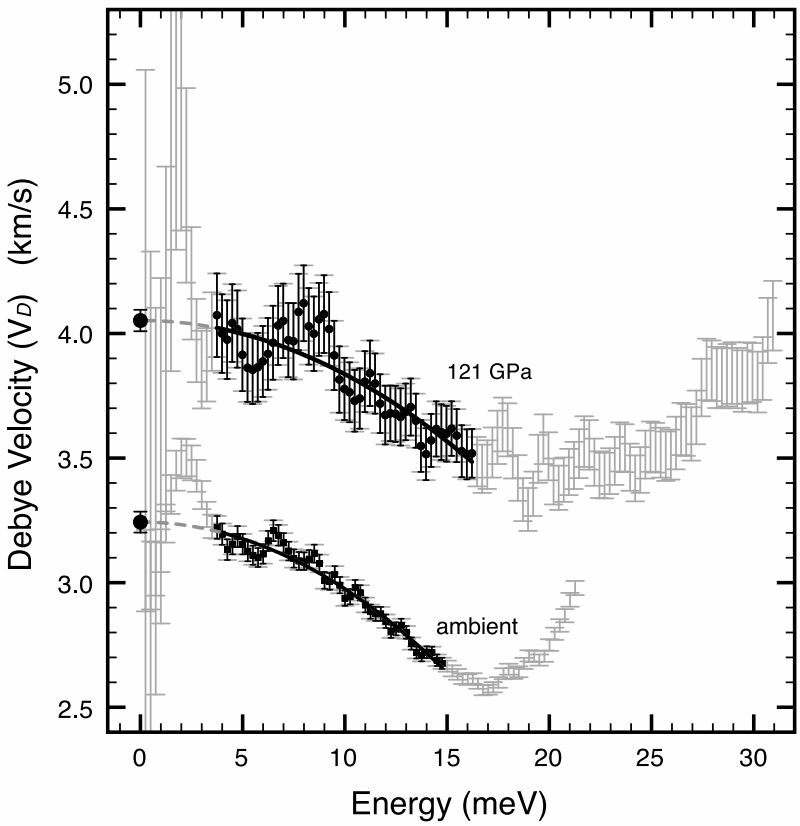

Figure 2.7: Determination of the Debye sound velocity of $(Mg_{.15}Fe_{.85})O$ at ambient pressure and 121 GPa. Symbols show values of Equation (2.1). Solid lines show the best fit of the empirical function $f(E)$ as explained in the text.

the fit procedure. Figure 2.7 shows $V(E)$, the fitted function $f(E)$, and the optimum value of V_D for ambient pressure and 121 GPa. Dashed lines illustrate the extrapolations using the best fits to obtain the Debye sound velocities.

In Figure 2.8, we plot V_D's determined for the entire pressure range. For comparison, we also show V_D's of $Fe_{.947}O$ that we determined from the PDOSs reported in a published NRIXS study, which was conducted at 300 K up to 49 GPa (*Struzhkin et al.*, 2001).

For an isotropic solid, V_D is related to the seismically relevant aggregate compressional (V_P) and shear (V_S) velocities by

$$3/V_D^3 = (1/V_P^3) + (2/V_S^3) \quad \text{and} \quad V_P^2 - (4/3)V_S^2 = K_{0S}/\rho = V_\phi^2 \tag{2.2}$$

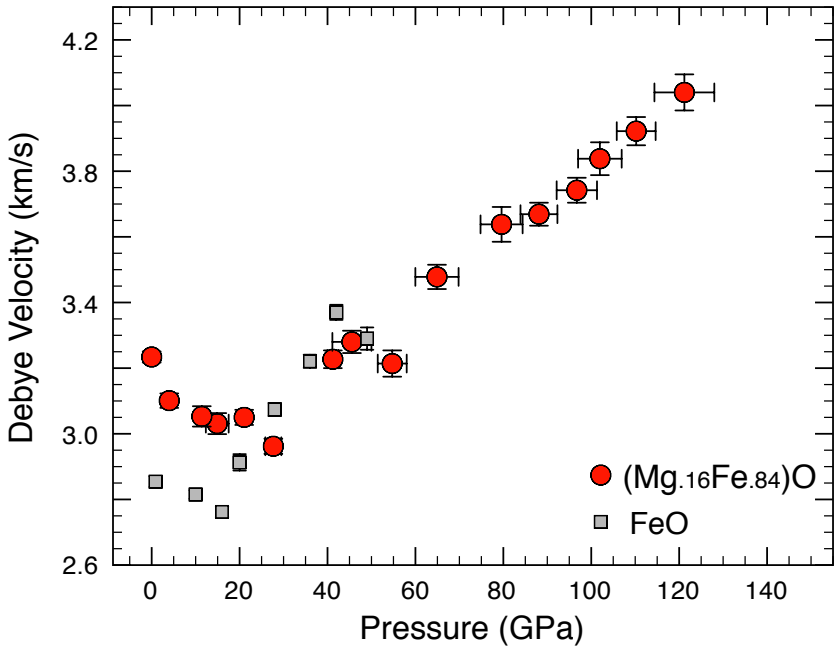

Figure 2.8: Debye sound velocities determined from the PDOS of $(Mg_{.16}Fe_{.84})O$ (this study) and of $Fe_{.947}O$ (*Struzhkin et al.*, 2001) at 300 K.

where K_{0S} is the adiabatic bulk modulus at ambient temperature, ρ is the density, and V_ϕ is the bulk sound velocity. K_{0S} is related to the isothermal bulk modulus, K_{0T}, by $K_{0S} = K_{0T}(1 + \alpha\gamma T)$. K_{0S} can be approximated by K_{0T}, because at room temperature $\alpha\gamma T \leq 0.01$ for most materials (*Angel and Jackson*, 2002). The isothermal third order Birch-Murnaghan weighted equation of state (EOS) from a high-pressure powder x-ray diffraction study up to 93 GPa on $(Mg_{.22}Fe_{.78})O$, a similar composition to that used in our NRIXS measurements, provided the values K_{0T}=191.2±5.5 GPa and K'_{0T}=2.5±0.1 (*Zhuravlev et al.*, 2010). The pressure-dependent density of $(Mg_{.16}Fe_{.84})O$ was obtained by rescaling this EOS with our initial density of 5.69(7) g/cm^3. X-ray diffraction spectra of our sample were taken at select pressures, including ambient, at the Advanced Light Source at Lawrence Berkeley National Laboratory, confirming our choice of EOS and pressure scale. The seismically relevant V_P and V_S values determined at each pressure point are shown for the entire pressure range (Figure 2.9, Table 2.1).

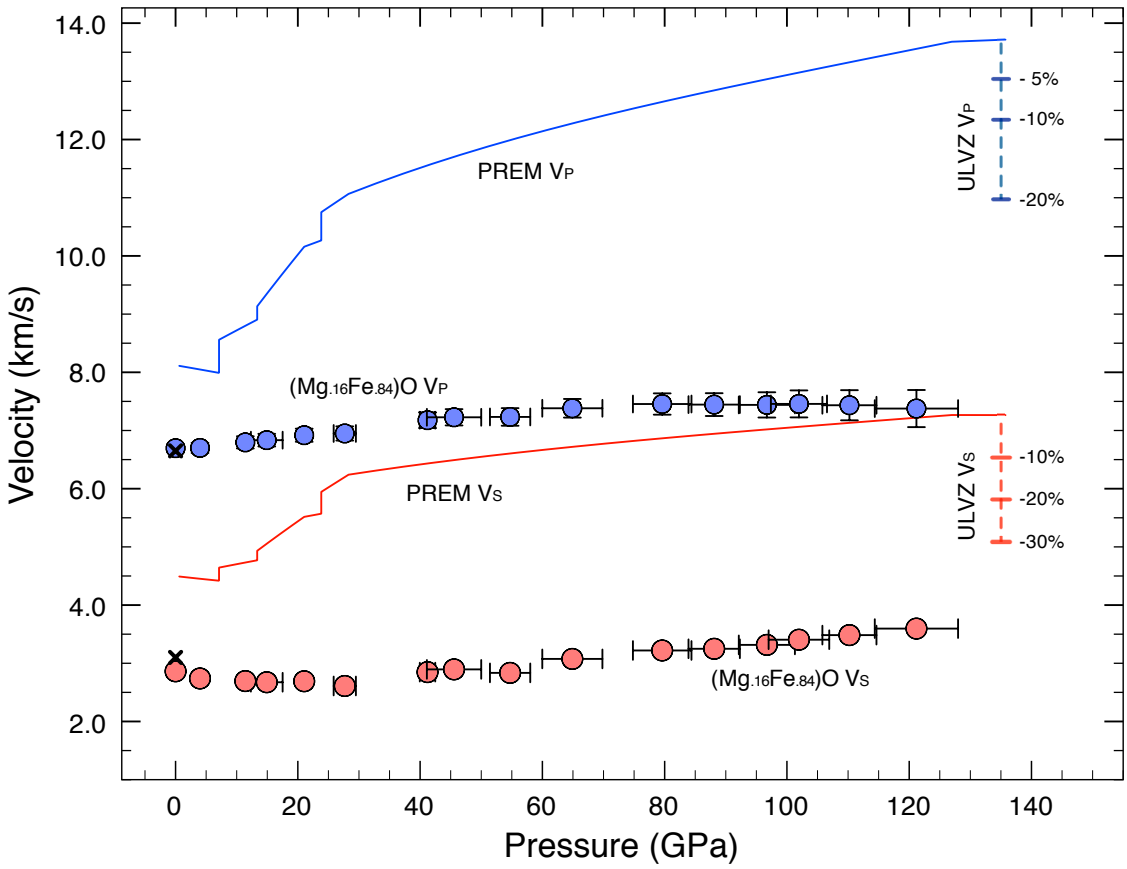

Figure 2.9: V_P (blue) and V_S (red), of $(Mg_{.16}Fe_{.84})O$ determined from V_D along with PREM (*Dziewonski and Anderson*, 1981) and ULVZs (*Thorne and Garnero*, 2004). ×: predicted sound velocities for $(Mg_{.16}Fe_{.84})O$ from an ultrasonic study on (Mg,Fe)O (*Jacobsen et al.*, 2002).

2.3 Results

At ambient pressure, the velocities of $(Mg_{.16}Fe_{.84})O$ are in good agreement with the trend in sound velocities for iron-rich (Mg,Fe)O (*Jacobsen et al.*, 2002; *Struzhkin et al.*, 2001, Figures 2.8, 2.9). In-situ synchrotron Mössbauer spectroscopy shows an absence of magnetic ordering (Figure 2.6) at low pressures, and detailed analysis reveals a quadrupole splitting of about 0.8 mm/s. At pressures approaching 28 GPa, both V_D and V_S of $(Mg_{.16}Fe_{.84})O$ decrease with increasing pressure (Figures 2.8, 2.9). The softening occurs in the vicinity of the transition from the paramagnetic state to a magnetically ordered state around 28 GPa (Figure 2.6). The presence of magnetic hyperfine fields is clear evidence for a magnetically ordered state demonstrating a magnetic transition in $(Mg_{.16}Fe_{.84})O$ around 28 GPa at 300 K—a finding in agreement with a conventional Mössbauer

Pressure (GPa)	Density (g/cm^3)	V_D (km/s)	V_P (km/s)	V_S (km/s)
0	5.69(7)	3.23(2)	6.70(9)	2.86(2)
4.0(3)	5.81(8)	3.10(2)	6.70(9)	2.74(2)
11.4(3)	6.02(8)	3.05(3)	6.8(1)	2.70(3)
15(3)*	6.1(1)	3.03(3)	6.8(1)	2.67(3)
21.0(4)	6.27(8)	3.05(2)	6.9(1)	2.69(2)
28(2)	6.44(9)	2.96(2)	6.9(1)	2.61(2)
41(1)	6.8(1)	3.23(2)	7.2(1)	2.85(2)
46(4)	6.9(1)	3.28(3)	7.2(1)	2.90(3)
55(3)	7.1(1)	3.21(4)	7.2(2)	2.84(3)
65(5)	7.4(1)	3.48(3)	7.4(2)	3.08(4)
80(5)	7.7(1)	3.64(5)	7.5(2)	3.22(5)
88(4)	7.9(1)	3.67(3)	7.5(2)	3.25(3)
97(5)	8.1(1)	3.74(3)	7.4(2)	3.32(3)
102(5)	8.2(2)	3.84(5)	7.5(2)	3.41(5)
110(4)	8.5(2)	3.92(2)	7.5(3)	3.48(4)
121(7)	8.7(2)	4.04(5)	7.4(3)	3.60(5)

Table 2.1: Summary of pressure, density, Debye sound velocity (V_D), and compressional (V_P) and shear (V_S) sound velocities of $(Mg_{.16}Fe_{.84})O$. Numbers in parenthesis reflect the error on the last digit. Errors in pressure reflect the standard deviation of pressures measured from multiple rubies surrounding the sample, measured before and after the x-ray measurement. Errors in ambient pressure density reflect the uncorrelated errors of unit cell volume measurement, sample composition, and assumed vacancies. Errors in V_D incorporate fitting errors in the low-energy region of the PDOS (Figure 2.7) as well as the propagation of the errors in density and pressure. This error is then propagated further to the V_P and V_S errors. * NaCl pressure medium.

study on $(Mg_{.20}Fe_{.80})O$ (*Speziale et al.*, 2005). A similar softening is observed for $Fe_{.947}O$ (*Struzhkin et al.*, 2001, Figure 2.9) and other iron-rich (Mg,Fe)O samples (*Jacobsen et al.*, 2004). This particular behavior has been associated with phonon-magnon coupling (*Struzhkin et al.*, 2001) and has been attributed to c_{44} mode softening preceding the B1 to rhombohedral structural distortion (*Mao et al.*, 1996).

At 121 GPa the fast oscillations, thus the magnetic hyperfine fields, disappear in the time spectrum (Figure 2.6), and is consistent with the onset of a spin transition into a low-spin state of the Fe 3*d*-electron configuration. We note that at pressures above 100 GPa, V_P ceases to increase and gradually softens. Such a behavior is consistent with a transition to a low spin state, as similar observations have been reported for iron-poor (Mg,Fe)O in the vicinity of a spin transition (*Crowhurst et al.*, 2008). Most important, the very low pressure derivatives of V_P and V_S for $(Mg_{.16}Fe_{.84})O$ above 28 GPa persist to the highest pressure measured and ensure that this material retains ultra-low sound velocities at core-mantle boundary pressures.

2.4 Ultralow-Velocity Zones

The shear sound velocity of $(Mg_{.16}Fe_{.84})O$ at 121 GPa is about 55% and 50% reduced compared to MgO (*Murakami et al.*, 2009) and the Preliminary Reference Earth Model (PREM) (*Dziewonski and Anderson*, 1981), respectively. The V_P/V_S ratio at the highest pressure measured is 2.1±0.1, which falls within the V_P/V_S range of ULVZs (2.2±0.3) (*Thorne and Garnero*, 2004). The Poisson ratios (ν) determined from seismic ULVZ observations range from 0.30 to 0.41 and compare favorably to our value of 0.34±0.02 for iron-rich (Mg,Fe)O at 121 GPa and 300 K.

At thousands of K and regardless of its structure (*Lin et al.*, 2003), $(Mg_{.16}Fe_{.84})O$ is unlikely to be stiffer than it is at room temperature, which could result in even lower sound velocities at the CMB. As an illustration of the expected V_P, V_S, and density of a mechanical mixture containing iron-rich (Mg,Fe)O and ambient mantle material, we estimate the effect of temperature on $(Mg_{.16}Fe_{.84})O$'s properties using MgO behavior as a proxy (*Sinogeikin et al.*, 2000). Due to the highly uncertain elastic properties of silicates under CMB conditions, we employ PREM as our bound for the remaining silicate fraction, while recognizing that PREM values may underestimate silicate behavior. We then calculate the Voigt-Reuss-Hill mechanical mixing envelopes for V_P, V_S, and density (*Watt et al.*, 1976) for a given vol% of $(Mg_{.16}Fe_{.84})O$ and PREM (Figure 2.10). To first order, mixing of just 12 vol% of $(Mg_{.16}Fe_{.84})O$ with 88 vol% silicates (represented here by PREM) matches signature seismic observations for the ULVZ (Figure 2.10).

While ULVZ provinces are often considered to be patches of dense partial melt, no measurements exist for the sound velocities of partially molten mantle material at CMB conditions. The connection between ULVZs and partial melting was popularized by the correlation between ULVZ and hot spot locations (*Williams et al.*, 1998). However, not all ULVZs are related spatially to hot spots. An alternative explanation of several ULVZ observations is a dense, localized solid layer containing some amount of iron-rich (Mg,Fe)O. A solid dense layer would not require the intersection of the local geotherm and solidus of the mantle and can produce low sound speeds independent of partial melting (Figure 2.10).

This scenario would require a mechanism in which the (Mg,Fe)O phase becomes enriched in iron

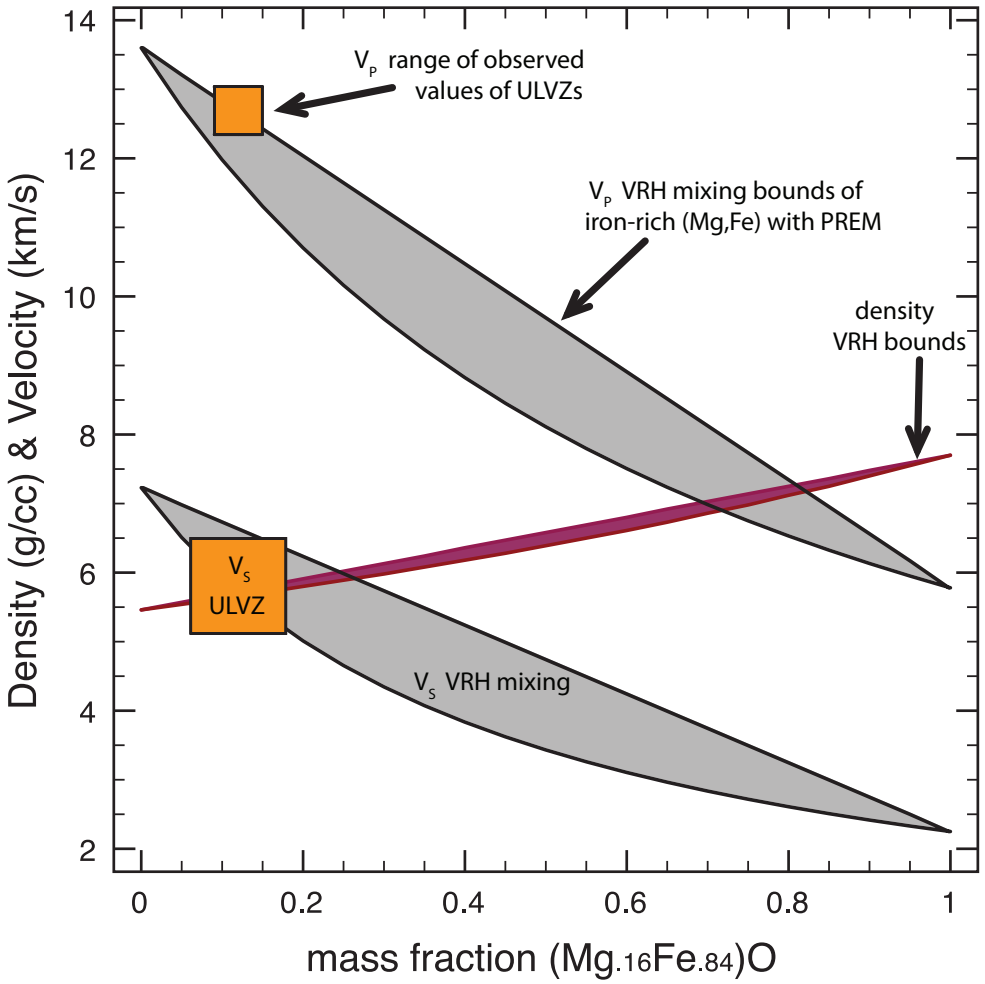

Figure 2.10: Voigt-Reuss-Hill (VRH) mixing of V_P, V_S, and density (red area) of $(Mg_{.16}Fe_{.84})O$ with PREM (see text for details). In orange boxes, we plot V_P and V_S of the ULVZ's centered at 12 vol% $(Mg_{.16}Fe_{.84})O$, which produces a ν of about 0.34. This particular calculation assumes a pressure of 123 GPa and a temperature of 2700 K. The widths of the ULVZ symbols are arbitrary.

in localized areas of the CMB. It has been suggested that extensive iron enrichment could localize in patches in the vicinity of the CMB due to viscosity variations, because liquid iron can be pulled up into the lower mantle on the km scale (*Kanda and Stevenson*, 2006). Iron-rich pockets could represent residue of a fractional crystallization of primordial magma ocean (*Labrosse et al.*, 2007). In representative mantle assemblages with typical amounts of iron, (Mg,Fe)O has been identified as the preferred iron sink (*Auzende et al.*, 2008; *Sinmyo et al.*, 2008).

Chemical reaction studies between liquid iron and lower mantle perovskite or oxide have produced

a wide range of results, leading to interpretations ranging from production of FeSi and FeO (*Knittle and Jeanloz*, 1991; *Song and Ahrens*, 1994) to dissolution of oxygen into liquid iron (*Takafuji et al.*, 2005; *Frost et al.*, 2010). Further investigations exploring the dependence of these reactions on CMB fugacity and chemistry may address these discrepancies, which could be complicated by the possibility of disequilibria. Nevertheless, the low sound velocities of iron-rich (Mg,Fe)O provide compelling motivation to explore the distribution of iron-rich (Mg,Fe)O in the core-mantle boundary region.